

Received December 8, 2020, accepted December 25, 2020, date of publication December 31, 2020, date of current version January 13, 2021.

Digital Object Identifier 10.1109/ACCESS.2020.3048418

Human-Robot Interaction Control for Robot Driven by Variable Stiffness Actuator With Force Self-Sensing

YINGHAO NING^{1,2}, YIFAN LIU^{1,2}, FENGFENG XI², KE HUANG³,
AND BING LI^{1,2,4}, (Senior Member, IEEE)

¹State Key Laboratory of Robotics and System (HIT), Harbin 150001, China

²School of Mechanical Engineering and Automation, Harbin Institute of Technology, Shenzhen 518055, China

³Shenzhen Cansing Technology Company Ltd., Shenzhen 518055, China

⁴Peng Cheng Laboratory, Shenzhen 518055, China

Corresponding authors: Fengfeng Xi (fengxi@ryerson.ca) and Ke Huang (k.huang@cansing.com)

This work was supported in part by the Key-Area Research and Development Program of Guangdong Province under Grant 2019B090915001, in part by the National Key Research and Development Program of China under Grant 2017YFB1302200, and in part by the Shenzhen Research and Development Program of China under Grant JSGG20180504170011639 and Grant JCYJ20200109112818703.


ABSTRACT Robots driven by variable stiffness actuators (VSAs) have been an important technology as they could provide intrinsic compliance for safe human-robot interaction. The internal compliance of VSA also makes it possible for the actuator to act as a torque sensor and estimate the external force. This paper presents a physical human-robot interaction control strategy for robots driven by VSA with force self-sensing. The VSA adopted in the robotic system improves the safe performance of physical human-robot interaction. The interaction force is directly estimated by measuring the internal deformation of VSA with a stiffness region control which ensures a better resolution of force estimation and avoids transgressing the limits of deformation simultaneously. Then an online estimation method for the human motion intention is developed to generate the desired trajectory based on the estimated force. The impedance control is designed to enable the robot to actively follow the desired trajectory with compliance. Under the proposed control strategy, the robot is capable of actively tracking the “motion intention” of human with the estimated interaction force, which is demonstrated through experiment studies.

INDEX TERMS Force self-sensing, motion intention estimation, physical human-robot interaction, variable stiffness actuator (VSA).

I. INTRODUCTION

In recent years, society has recognized the significance of robots in assisting human motions, such as reducing workload, improving the efficiency, enhancing the productivity, rehabilitation therapy, and so on. Safety is a critical consideration in these applications where involves direct physical human-robot interaction. Using flexible actuators is a popular solution for the safe cooperation, since they provide several attractive characteristics such as low output impedance, back drivability and shock tolerance [1], [2].

Flexible joints use springs or other flexible components to decouple the motor from the environment motion thus

The associate editor coordinating the review of this manuscript and approving it for publication was Yingxiang Liu .

improving the safe performance. Since their introduction, flexible joints have been utilized in different kinds of robotic applications including rehabilitation robots [3]–[7], walking robots [8], humanoids [9], [10] and haptics [11], [12]. According to whether the joint involves the stiffness regulation, flexible joint can be divided into two categories: series elastic actuator (SEA) and variable stiffness actuator (VSA). For SEA, the compliant component is directly in series-elastic configuration to provide internal compliance. However, the physical compliance of SEAs is fixed which weakens the achievable bandwidth of actuator. On the contrary, as the stiffness of VSAs could be regulated, VSAs are capable of surmounting the bandwidth limitation and enhancing the task adaptability to different kind of environments [13], [14]. Therefore, VSA is more suitable for the

interaction control which involves the environment uncertainties and dynamically changing in the process of human robot interaction.

Before performing the human-robot interaction, the motion intention of human should be identified firstly. Much research efforts were dedicated to the biological signals, such as skin electromyography (EMG) [15] and electroencephalography (EEG) [16], to estimate the motion intention of human. Nevertheless, it is time-consuming to attach or detach sensors to or from the muscles of human when utilizing these biological signals resulting in inconvenience. Besides, these biological signals require higher concentration of subjects' attention, and these signals would be affected by the individual difference. Another medium for motion intention estimation is the interaction force. As the signals of interaction force are relatively robust, the interaction force between the robot and human is also widely utilized for the motion estimation. In [17], [18], the motion intentions were recognized by the difference between the estimated and measured torque of robots. However, such approach requires the accurate dynamics of robots and human arms or legs. Velocity-based admittance controllers [19], [20] were developed for identifying the motion intention of human by changing the damping variable. Nevertheless, the variable stiffness property is not considered and the motion intention estimation may not be accurate enough. In [21], the impedance model was utilized for estimating the motion intention by incorporating a neural network to display the relationship between the desired motion and interaction force. However, there are many undetermined parameters of neural network needed to be updated, leading to huge computation cost. This paper aims for a relatively accurate estimation of motion intention through the medium of interaction force with as few unknown parameters as possible.

When the interaction force is utilized to estimate the motion intention, special considerations should also be taken into account for the approach of detecting the interaction force. Traditionally, the forces are measured or estimated by detecting the signals of force sensor [3], [21], [22] and the current of motor [4]. Nevertheless, the former requires the expensive force sensor mounted onto the robot and the latter relies on the accurate dynamic models. Flexible actuator has the potential to estimate the external forces by only measuring the internal deflection of the compliant component, with no need for additional force sensor or accurate internal dynamics. For SEA whose stiffness is generally constant, it is compression spring [23], [24] or torsion spring [25] that converts the elasticity into force. However, it requires special consideration on selecting the stiffness of springs: the higher stiffness extends the range of allowable maximum force but results in a worse resolution of force estimation; the lower stiffness brings a better resolution of force estimation, but weakens the allowable maximum force considering the same maximum compression. Besides, the "softer" spring leads to a lower bandwidth which is not suitable for input signals with higher frequency. For VSA, the stiffness is changeable

and the internal compliance could be utilized for external force estimation [13], [26]. Since the stiffness is adjustable, the VSA has the potential to achieve a better resolution of force estimation and avoid violating the limitation of internal deflection simultaneously. However, little attention has been paid to such area.

In this paper, a control strategy for physical human-robot interaction is presented for robots driven by VSA. The basic design of VSA has been introduced in [27]. The goal of this paper is to propose and validate a controller to achieve an effective human-robot interaction that enables the robot to actively follow the motion intention of human. The motion intention is achieved through the medium of interaction force which is directly estimated by measuring the internal deflection of VSA. When realizing the "force self-sensing", a stiffness region control is developed, based on the improved Barrier Lyapunov function, to achieve a better resolution of force estimation and avoid violating the maximum internal deflection simultaneously. Besides, the motion intention is generated by estimating the dynamic model of upper limb which involves minimizing the interaction force between the human and robot. Different with the approach in [21] where the neural network was utilized, the unknown parameters needed to be updated in this paper are only the upper-limb dynamic models, thereby contributing to a lower computation cost. The impedance control is integrated into the controller to enable the robot to "actively" follow the desired motion with compliance. Finally, experiments are conducted to verify the effectiveness of the proposed controller.

The rest of this paper is organized as follows. In Section II, the robotic system is introduced. In Section III, the controller design is described in details. Section IV gives the experimental results. Discussions and concluding remarks are given in Section V and Section VI respectively.

II. ROBOTIC SYSTEM

The schematic of human-robot interaction and the VSA-actuated robot are shown in Fig. 1. The subject is asked to put their arm in the horizontal position and the upper limb is constrained to make cyclical abduction/adduction movement along the rotation axis of the robot. The dynamic modeling of human is simplified only considering the stiffness and damper parameters and the interaction force F_h by the human "pushes" the robot to follow the "motion intention".

A. MECHANICAL DESIGN OF VSA

The principle of VSA and its three-dimensional model can be seen in Fig. 2. The VSA is powered by two brush DC motors for the position control and stiffness regulation respectively, each of which has a rotary encoder. The stiffness regulation is realized by a lever mechanism which consists of the lever, pivot and springs. The position motor, shown as Motor1, transmits its motion firstly to the connecting disk on which the pivot and spring module are mounted, then to the lever through the pivot and spring module, and finally to output shaft. The motion of stiffness regulation motor, shown as

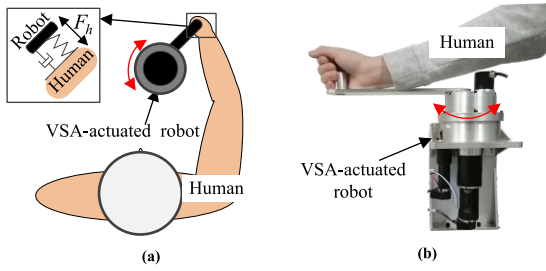


FIGURE 1. The schematic of human-robot interaction. (a) Top-down schematic view. (b) Human performing the task.

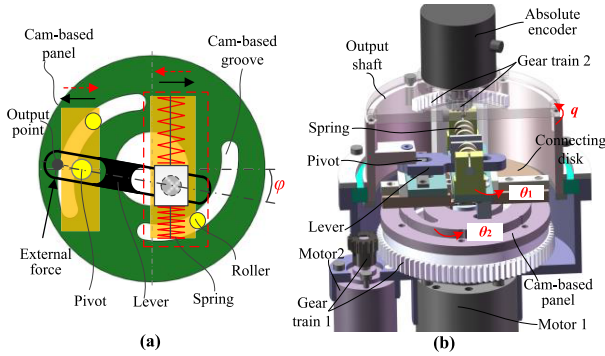


FIGURE 2. The structure of VSA. (a) Principle of the actuator. (b) Partial cross-sectional view of the actuator.

Motor2, is firstly transmitted to the gear train1 then to the cam-based panel. When regulating the stiffness, the locations of pivot and spring module are changed towards or away from the center of actuator simultaneously through the rotation of cam-based panel. When the external force is exerted onto the output shaft, the springs are compressed to generate force against the external force, thus introducing the compliance. One additional absolute encoder is installed to measure the internal deflection through gear train2. More details of the VSA can be found in [27].

The dynamic model of the VSA-driven robot can be expressed as:

$$\begin{cases} J_1 \ddot{\theta}_1 + K(\theta_1 - q) + f_{dis1} = \tau_1 \\ J_2 \ddot{\theta}_2 + f_{dis2} = \tau_2 \\ M \ddot{q} + C(q, \dot{q}) \dot{q} + G(q) + Kq = K\theta_1 + \tau_e \end{cases} \quad (1)$$

where J_1 and J_2 are inertias of Motor1 with connecting components, and Motor2 with its connecting components respectively; τ_1 and τ_2 denote the input torque exerted from Motor1 and Motor2 respectively; f_{dis1} and f_{dis2} are the non-linear friction for different modules respectively when regulating the stiffness; q is the position of output shaft, θ_1 is the position of connecting disk directly driven by Motor1, θ_2 is the position of cam-based panel actuated by Motor2, φ is the internal deflection angle and $q = \theta_1 + \varphi$; M , $C(q, \dot{q}) \dot{q}$ and $G(q)$ denote the inertia parameter, the centripetal and Coriolis torque, and the gravitational torque of the robot respectively; K is the stiffness of the actuator, and τ_e is the interaction force.

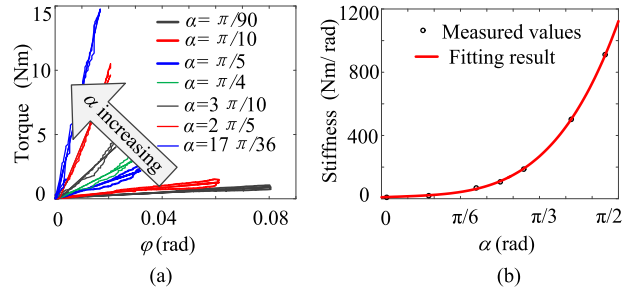


FIGURE 3. Results of stiffness calibration. (a) The relationship between the torque and deflection angle. (b) Fitting results of stiffness.

As the nonlinear friction exists when regulating the stiffness, the motions of motors are realized by servo drivers for a better position-tracking performance. Therefore, the dynamics of Motor1 and Motor2 are not concerned in this paper.

B. PERFORMANCE ANALYSIS OF FORCE SELF-SENSING

The stiffness is an essential parameter for force self-sensing which directly affects the resolution of force estimation. The details of stiffness analysis can be found in [27]. For the VSA, the stiffness is approximately constant for a specific α , where $\alpha = \theta_1 - \theta_2$. Besides, the stiffness calibration is also conducted to achieve an accurate relationship between the internal deflection and external force, shown in Fig. 3. Fig. 3(a) displays the original data depicting the relationship between the torque and internal deflection. The fitting result of stiffness calibration is shown in Fig. 3(b). The fitting result can be expressed as a polynomial function expressed by (2), where the order is constrained by the error sum of squares and the positive derivative of stiffness.

$$K = 9.40 + 33.12\alpha - 8.21\alpha^2 + 50.78\alpha^3 + 140.10\alpha^4 \quad (2)$$

where $\alpha = \theta_1 - \theta_2$.

From (2), the external force can be estimated by (3).

$$\tau_e = K\varphi \quad (3)$$

For a VSA with the lever mechanism for stiffness regulation, the maximum deflection angle φ_m and maximum operating torque τ_{em} are usually changeable according to different stiffness. When an external torque is exerted onto the actuator, it is required that the springs are compressed within allowable range and the external torque could not exceed the nominal value. Such demands are also found in literature [28].

Considering the VSA adopted in this paper, the designing constraints are given as [27]: (i) the compression of spring is less than 6 mm; (ii) the nominal torque of the actuator is 20 Nm which is related to the nominal torque of motors and the strength of internal parts. The maximum deflection angle φ_m and maximum operating torque τ_{em} can be obtained through simulation, the results of which are seen in Fig. 4.

As the results of Fig. 4 are obtained through simulation with several inequality constraints, it is difficult to achieve

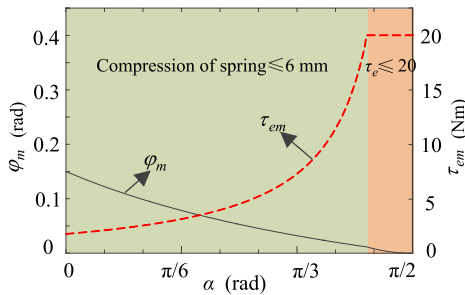


FIGURE 4. Maximum angular deflection and maximum operating torque.

explicit expressions for these constraints, thus inconvenient for the controller design. Therefore, data fitting method is utilized to display the relationships shown in Fig. 4. As there is a relationship between φ_m and τ_{em} , depicted by (3), only the relationship between τ_{em} and α is fitted, which is expressed by (4), and the maximum deflection angle φ_m can be calculated directly from (3).

$$\tau_{em} = \begin{cases} 1.691e^{1.2347\alpha} + 0.0013e^{6.6406\alpha}, & 0 \leq \alpha \leq 1.3587 \\ 20, & 1.3587 < \alpha \leq \pi/2 \end{cases} \quad (4)$$

When estimating the external force by the internal compliance of VSA, the resolution of the force estimation is determined by the joint stiffness and the resolution of encoder. When the resolution of encoder is decided, a higher stiffness leads to a worse resolution of force estimation. Hence, the lower stiffness is desired in the process of force estimation. Besides, the lower stiffness also contributes to the performance of safe human-robot interaction. Nevertheless, as shown in Fig. 3-4, the lower stiffness usually results in a smaller value of τ_{em} , which makes it easier to reach or transgress the maximum operating torque τ_{em} than a higher stiffness. Therefore, the stiffness of the VSA should be properly regulated while ensuring that the maximum operating torque τ_{em} is not violated and that the stiffness is lower properly for a better resolution of force estimation.

III. CONTROLLER DESIGN

In this section, the control strategy for physical human-robot interaction is developed for the robot driven by VSA. Even though the controller in this paper is only considering the robot with one degree of freedom (DOF), such controller is easily extended to robots with multi-DOFs. The controller consists of the stiffness region control, the estimation of human motion intention and the impedance control. The stiffness region control is to regulate the stiffness to achieve a better resolution and avoid violating the maximum operating torque. The human motion intention is estimated to generate the desired trajectory and the impedance control is implemented to drive the robot to “actively” track the desired trajectory with compliance. The block diagram of the control structure is shown in Fig. 5.

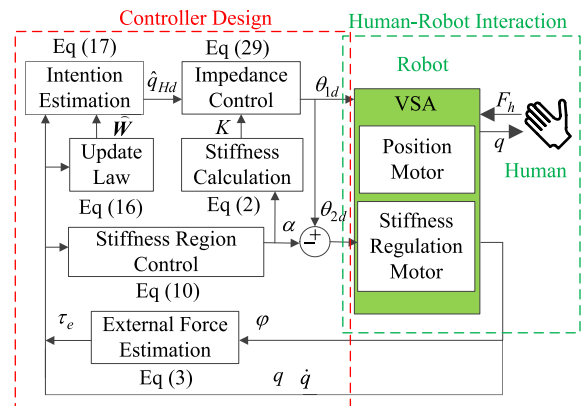


FIGURE 5. A block diagram of the control strategy.

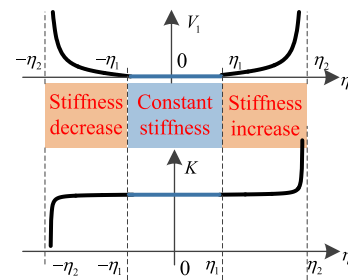


FIGURE 6. Schematic illustration of the improved barrier Lyapunov function.

A. STIFFNESS REGION CONTROL

As mentioned in Section II, the performance of force estimation is highly dependent on the stiffness of VSA. To improve the performance of force estimation, the stiffness regulation is specified as three regions, i.e., the constant stiffness region, stiffness increase region and stiffness decrease region. The objective is to make the stiffness stay within the constant stiffness region, where enables a proper resolution of force estimation and ensures that the interaction force would not transgress the maximum operating torque. The Barrier Lyapunov Function is a potential tool to handle the problem of region control [29]. To formulate the stiffness control method, an improved Barrier Lyapunov Function is proposed as:

$$V_1 = \frac{1}{2} \log \frac{(\eta_2 - \eta_1)^2}{(\eta_2 - \eta_1)^2 - [\max(0, |\eta| - \eta_1)]^2} \quad (5)$$

where $\eta = \frac{|\tau_e|}{\tau_{em}} - \eta_0$; η_0 , η_1 and η_2 are positive constants and $\eta_0 = \eta_2 > \eta_1$.

The η is developed with a η_0 to make the η symmetric about zero. As the range of $|\tau_e|/\tau_{em}$ is [0, 1], it is defined that $\eta_0 = \eta_2 = 0.5$ to make η within $[-0.5, 0.5]$. The η_1 is designed properly to construct a constant stiffness region that $|\tau_e|/\tau_{em}$ is within $[\eta_0 - \eta_1, \eta_0 + \eta_1]$.

An illustration of the improved Barrier Lyapunov Function is shown in Fig. 6. The range of constant stiffness region is highly influenced by the η_1 . When $\eta > \eta_1$, the $|\tau_e|/\tau_{em}$ transgresses the constant stiffness region and the external force τ_e

is reaching or violating the maximum operating torque τ_{em} . Within such region, the stiffness is required to increase so that the maximum torque τ_{em} grows until the η returns back to the constant stiffness region. When $\eta < -\eta_1$, the $|\tau_e|/\tau_{em}$ is closer to 0 and the stiffness is controlled to decrease for a better resolution of force estimation until the η goes back to the constant stiffness region. In the constant stiffness region where the η is within $[-\eta_1, \eta_1]$, the stiffness keeps invariant as the $|\tau_e|$ is far away from the maximum operating torque and the stiffness is lower for a better resolution of force estimation.

As the function V_1 has several regions, the derivative of V_1 is given by

$$\dot{V}_1 = \begin{cases} 0, & |\eta| \leq \eta_1 \\ \frac{(\eta - \eta_1) \dot{\eta}}{(\eta_2 - \eta_1)^2 - (\eta - \eta_1)^2}, & \eta_1 \leq \eta \leq \eta_2 \\ \frac{(\eta + \eta_1) \dot{\eta}}{(\eta_2 - \eta_1)^2 - (\eta + \eta_1)^2}, & -\eta_2 \leq \eta \leq -\eta_1 \end{cases} \quad (6)$$

In order to constrain the η within $[-\eta_1, \eta_1]$, it is required that $\dot{V}_1 \leq 0$. Design the $\dot{\eta}$ as:

$$\dot{\eta} = \begin{cases} 0, & -\eta_1 \leq \eta \leq \eta_1 \\ -k_\eta (\eta - \eta_1), & \eta_1 \leq \eta \leq \eta_2 \\ -k_\eta (\eta + \eta_1), & -\eta_2 \leq \eta \leq -\eta_1 \end{cases} \quad (7)$$

where k_η is the positive constant, which affects the rate of stiffness regulation. Substituting (7) into (6) yields $\dot{V}_1 \leq 0$.

From the definition of η in (5), the derivate of η is expressed by

$$\dot{\eta} = -\frac{|\tau_e|}{\tau_{em}^2} \dot{\tau}_{em} = -\frac{|\tau_e|}{\tau_{em}^2} \frac{d\tau_{em}}{d\alpha} \dot{\alpha} \quad (8)$$

Combining (7) and (8), the derivative of α is expressed as:

$$\dot{\alpha} = \begin{cases} 0, & -\eta_1 \leq \eta \leq \eta_1 \\ k_\eta (\eta - \eta_1) \frac{\tau_{em}^2}{|\tau_e|} \frac{1}{d\tau_{em}/d\alpha}, & \eta_1 \leq \eta \leq \eta_2 \\ k_\eta (\eta + \eta_1) \frac{\tau_{em}^2}{|\tau_e|} \frac{1}{d\tau_{em}/d\alpha}, & -\eta_2 \leq \eta \leq -\eta_1 \end{cases} \quad (9)$$

For a discrete-time implementation, α can be expressed as:

$$\alpha(t_{k+1}) = \alpha(t_k) + \dot{\alpha}(t_k) \times \Delta t \quad (10)$$

where $t_{k+1} = t_k + \Delta t$ and Δt is the sampling period.

From (2), the stiffness K could be regulated by the change of α in (10), thereby realizing the stiffness region control.

Remark 1: It is highly possible that the interaction force τ_e is close to zero at the beginning or some certain moments in the process of human-robot interaction. In the practical implementation, a minimum stiffness is set in case that the stiffness keeps dropping to zero when the τ_e is around a small value.

B. MOTION INTENTION ESTIMATION

The objective of the motion intention estimation is to generate the desired trajectory that would be followed by robot. As discussed in [30], the model of upper limb is mainly affected by the damper and spring parameters. Therefore, the human model can be simplified as

$$-C_H \dot{q} + G_H (q_{Hd} - q) = \tau_e \quad (11)$$

where C_H and G_H are the damper and spring variables of the human limb respectively, and q_{Hd} is the desired trajectory reflecting the motion intention of the human.

By (11), the motion intention can be expressed as

$$q_{Hd} = q + Y^T W \quad (12)$$

where $Y(t) = [\tau_e \dot{q}]^T$, $W(t) = [w_1 w_2]^T = [1/G_H C_H/G_H]^T$.

As parameters C_H and G_H are unknown in the human-robot interaction, the motion intention q_{Hd} can be estimated as:

$$\hat{q}_{Hd} = q + Y^T \hat{W} \quad (13)$$

where $\hat{W}(t) = [\hat{w}_1 \hat{w}_2]^T$.

The objective is to minimize the interaction force τ_e as much as possible, which diminishes the discrepancy between the predicted motion and the real one. Therefore, an energy function of τ_e is developed and the \hat{W} is regulated online towards the steepest descent direction of the energy function. The energy function is given by:

$$E = \frac{1}{2} \tau_e^2 \quad (14)$$

Combining (13) and (14), the update law of \hat{W} is obtained as:

$$\begin{aligned} \dot{\hat{W}}(t_k) &= -\Gamma_0 \frac{\partial E}{\partial \hat{W}} = -\Gamma_0 \frac{\partial E}{\partial \tau_e} \frac{\partial \tau_e}{\partial \hat{q}_{Hd}} \frac{\partial \hat{q}_{Hd}}{\partial \hat{W}} \\ &= -\Gamma_0 \tau_e \frac{1}{\hat{w}_1} Y \end{aligned} \quad (15)$$

where $\Gamma_0 \in \mathfrak{R}^{2 \times 2}$ is a constant, positive and diagonal matrix. Even though $1/\hat{w}_1$ is time varying, it can still be absorbed by Γ_0 for the simplification and such absorption has little effect on the results. Therefore, the update law of \hat{W} can be expressed as:

$$\dot{\hat{W}}(t_k) = -sgn(\hat{w}_1) \tau_e(t_k) \Gamma_0 Y(t_k) \quad (16)$$

where $sgn(\hat{w}_1) = \begin{cases} 1, & \hat{w}_1 \geq 0 \\ -1, & \hat{w}_1 < 0 \end{cases}$.

Therefore, the estimation of q_{Hd} is given as

$$\begin{aligned} \hat{q}_{Hd}(t_{k+1}) &= q(t_{k+1}) \\ &+ Y^T(t_{k+1}) \left[\hat{W}(t_k) + \dot{\hat{W}}(t_k) \times \Delta t \right] \end{aligned} \quad (17)$$

On the basis of the previous discussions, the human motion intention can be estimated through (17).

C. IMPEDANCE CONTROL

With the available desired trajectory of (17), the impedance control is adopted to make the robot move towards the desired position with compliance, thus improving the performance of safe human-robot interaction. The impedance model is defined as:

$$M_d (\ddot{q} - \ddot{q}_d) + C_d (\dot{q} - \dot{q}_d) + G_d (q - q_d) = \tau_e \quad (18)$$

where $q_d = \hat{q}_{Hd}$, and M_d , C_d and G_d are the desired inertia, damping and stiffness respectively.

By defining the position error as $e = q - q_d$ and constructing an error signal $w = M_d \ddot{e} + C_d \dot{e} + G_d e - \tau_e$, the control objective of the impedance model is to make $\lim_{t \rightarrow \infty} w(t) = 0$.

An augmented impedance error is given by:

$$\bar{w} = \ddot{e} + (\Lambda_1 + \Gamma_1) \dot{e} + \Lambda_1 \Gamma_1 e - (\dot{f}_i + \Gamma_1 f_i) \quad (19)$$

where $\Lambda_1 + \Gamma_1 = M_d^{-1} C_d$, $\Lambda_1 \Gamma_1 = M_d^{-1} G_d$, $\dot{f}_i + \Gamma_1 f_i = M_d^{-1} \tau_e$, Λ_1 and Γ_1 are positive parameters.

In fact, the parameters Λ_1 and Γ_1 can be obtained by

$$\Gamma_1 = \frac{M_d^{-1} C_d \pm \sqrt{M_d^{-2} C_d^2 - 4M_d^{-1} G_d}}{2} \quad (20)$$

$$\Lambda_1 = \frac{M_d^{-1} C_d \mp \sqrt{M_d^{-2} C_d^2 - 4M_d^{-1} G_d}}{2} \quad (21)$$

For a discrete-time implementation, it is reasonable to define that $\dot{f}_i(t_{k+1}) = [f_i(t_{k+1}) - f_i(t_k)] / \Delta t$, where $t_{k+1} = t_k + \Delta t$ and Δt is the sampling period. Then $f_i(t_{k+1})$ can be expressed as

$$f_i(t_{k+1}) = \frac{f_i(t_k) + \Delta t M_d^{-1} \tau_e(t_{k+1})}{1 + \Delta t \Gamma_1} \quad (22)$$

By defining

$$z = \dot{e} + \Lambda_1 e - f_i \quad (23)$$

It can be obtained that

$$\bar{w} = \dot{z} + \Gamma_1 z \quad (24)$$

The z can be viewed as a low-pass-filtered signal with respect to \bar{w} . It is reasonable to derive that the convergence of $z \rightarrow 0$ will lead to $\bar{w} \rightarrow 0$. Therefore, the control objective $\lim_{t \rightarrow \infty} w(t) = 0$ finally becomes:

$$\lim_{t \rightarrow \infty} z = 0 \quad (25)$$

An augmented state variable is defined as

$$\dot{q}_r = \dot{q}_d - \Lambda_1 e + f_i \quad (26)$$

Combining (23) and (26), it can be derived as

$$z = \dot{q} - \dot{q}_r \quad (27)$$

By using (27), the third equation of (1) is rewritten as

$$M \dot{z} + M \dot{q}_r + C(q, \dot{q}) \dot{q} + G(q) + Kq = K\theta_1 + \tau_e \quad (28)$$

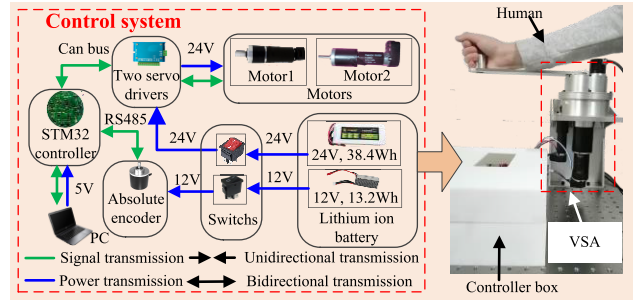


FIGURE 7. Experimental setup and its control system.

Then the desired input of the robot dynamics can be developed as:

$$\theta_{1d} = q + \frac{1}{K} [-k_z z + M \ddot{q}_r + C(q, \dot{q}) \dot{q} + G(q) - \tau_e] \quad (29)$$

where k_z is a positive parameter.

The desired input of the stiffness regulation motor is given as:

$$\theta_{2d} = \theta_{1d} - \alpha \quad (30)$$

where α is described as (10).

Substituting (29) into (28), it can be derived $M \dot{z} = -k_z z$. Therefore, considering the robot dynamics given by (1), the desired input (29) guarantees the result that $\lim_{t \rightarrow \infty} z = 0$.

Remark 2: In the practical implementation, the interaction force τ_e is deemed to be zero in the control strategy if it is smaller than a certain value in order to improve the system robustness. This prevents the system from suffering some unknown disturbances of interaction force, thus making the system more stable.

IV. EXPERIMENT

In this section, the proposed control strategy is implemented through experiments. Fig. 7 illustrates the experimental setup and its control system. The VSA-actuated robot is mainly made up with a robot link driven by VSA. In the control system, the hardware consists of a STM32-based controller, two servo drivers, two motors, an absolute encoder, lithium ion batteries, switches and a laptop. The servo drivers are utilized to collect and send signals from and to motors for position control. The STM32-based controller is to execute the control algorithm, handle the signals transmitted from servo drivers and absolute encoder, then send the control commands to servo drivers. The reason for using STM32-based controller is that it is convenient to realize the RS485 bus with low cost. The detailed signal and power transmissions can be seen in Fig. 7.

The goal of experiments is to verify the effectiveness of proposed strategy. The subject is asked to put their arm in the horizontal position and the upper limb is constrained to make a cyclical abduction/adduction movement along the rotation axis of the robot, shown in Fig. 1. The interaction force is estimated by measuring the internal deflection of

VSA. In experiment, the interaction force is perceived as the motion intention and then the robot drives the upper limb to “actively” track the desired “motion intention”.

To better display the effectiveness of stiffness region control, two different experiments are conducted with different initial stiffness. In the first case, one higher initial stiffness is selected, which is $\alpha = \pi/4$, to verify the stiffness regulation from stiffness decrease region to constant stiffness region. In the second case, one smaller initial stiffness is pre-established, which is $\alpha = \pi/18$, to verify that stiffness could increase when it is within the stiffness increase region. Additionally, one additional torque sensor is utilized to further verify the accuracy of force estimation in a dynamic condition.

In the experiments, the time period is set as $t_f = 50s$. The parameters in the improved Barrier Lyapunov Function (5) and (7) are set as: $\eta_1 = 0.3, k_\eta = 0.4$. This makes a constant stiffness region that $|\tau_e|/\tau_{em}$ is within $[0.2, 0.8]$. The parameters in (15) are set as $\Gamma_0 = \begin{bmatrix} 0.05 & 0 \\ 0 & 0.05 \end{bmatrix}$. The desired impedance parameters in (18) are set as $M_d = 0.1, C_d = 0.8, G_d = 0.375$. Two parameters Λ_1 and Γ_1 in (19) are specified as: $\Lambda_1 = 0.5, \Gamma_1 = 7.5$. The parameter of desired position control input (29) is set as $k_z = 1.0$. Parameters k_η, Γ_0 and k_z are tuned in practice, while η_1 and impedance parameters, correlated with the constant stiffness region and interaction force respectively, are selected based on the practical necessity.

In the experiment, a minimum stiffness is set as $\alpha = \pi/12$ in case that the stiffness keeps dropping to zero when the τ_e is around a small value. The minimum stiffness is decided with the consideration of the range of interaction force through (2)-(3). It is not recommended to set the minimum stiffness too low since the lower minimum stiffness results in that the stiffness easily reaches the minimum limit thus making damages to the actuator. Besides, the threshold of the interaction force discussed in Remark 2 is selected as 0.2 Nm to enhance the stability of the system, where only the forces exceed the threshold are considered in the experiment. The threshold is decided according to the range of interaction force when the object performs the task.

Fig. 8 shows the experimental results of the first case. In Fig. 8 (a), it can be seen that there is little error between the desired position and the actual position of the robot, which indicates that the robot follows the human motion intention “actively” with the proposed control strategy. Such better tracking performance also indirectly verifies the efficacy of the proposed force estimation method. From the partial enlarged part, the desired position is bouncing up and down around the actual position. Such phenomenon can be explained by the oscillation property of the \hat{W} shown in Fig. 8 (b). Fig. 8 (c)-(d) show the performance of stiffness region control. The stiffness decreases at $t \approx 13s$ as the $|\tau_e|/\tau_{em}$ is smaller than 0.2 indicating the stiffness can be still be reduced for a better resolution of force estimation. Therefore, the stiffness keeps decreasing for enhancing the

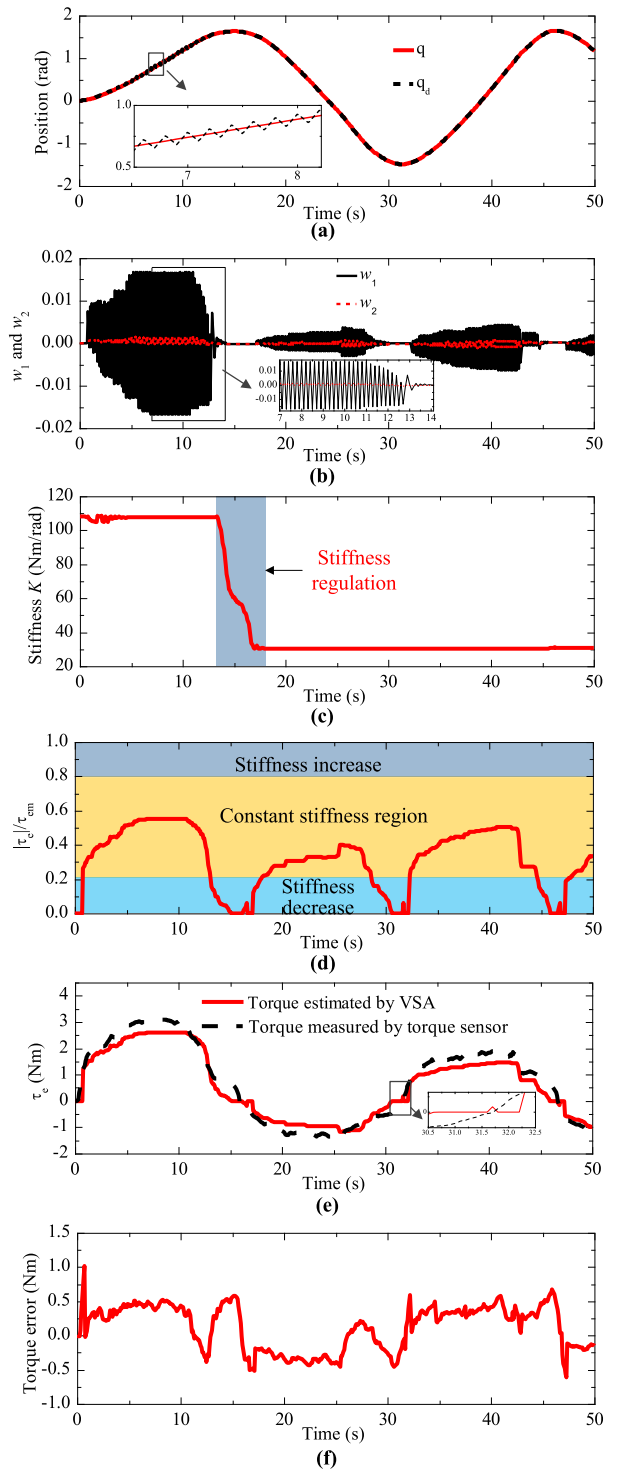


FIGURE 8. Experimental results with initial stiffness of $\alpha = \pi/4$.

resolution performance of force estimation until the $|\tau_e|/\tau_{em}$ goes back to the constant stiffness region. The performance of the accuracy for force estimation by VSA can be seen in Fig. 8 (e)-(f). It is clearly found that most errors between the torque measured by torque sensor and the torque estimated by VSA are within $[-0.5, 0.5]$ and the maximum

error is less than 1 Nm. As observed, the proposed force estimation method displays an excellent performance with a higher accuracy and the estimated torque is acceptable in the human-robot interaction.

The experimental results with an initial stiffness of $\alpha = \pi/18$ can be seen in Fig. 9. Similar with the stiffness of $\alpha = \pi/4$, the robot could “actively” follow the human motion intention with little error between the desired position and the actual position, as shown in Fig. 9 (a)-(b). From Fig. 9 (c)-(d), it is clearly found that the initial stiffness is so small that the interaction force is violating the maximum operating torque at $t \approx 3 - 9s$. Hence the stiffness is controlled to increase for dragging the $|\tau_e|/\tau_{em}$ back into the constant stiffness region. In Fig. 9 (e)-(f), it can be seen that the estimated force could be well applied in the physical human-robot interaction with a higher accuracy.

The oscillations, shown in Fig. 8 (b) and Fig. 9 (b), can be explained by the updating law in Section III B. The update law is generated by minimizing the interaction force with the gradient descent method. It is commonly accepted that parameters converge to the optimum with “zigzag” shape when utilizing the gradient descent method. Furthermore, according to (16), the degree of oscillation is related to the torque τ_e and the velocity \dot{q} . Hence, the larger torque and velocity would bring heavier oscillations.

From Fig. 8(e) and Fig. 9(e), there are periods that the estimated force by VSA is zero while the torque measured by torque sensor is not zero, shown as the partial enlarged parts. That is because the interaction force is deemed to be zero in the control strategy, if it is smaller than a certain value, as depicted in Remark 2. The normal values of interaction force can be depicted through the torque measured by torque sensor to make a comparison. Such phenomena occur when the actuator changes the rotation from one direction to another in the experiment.

From Fig. 8 (c)-(d) and Fig. 9(c)-(d), there are some periods that the stiffness remains constant even when the $|\tau_e|/\tau_{em}$ is below 0.2. The reason is that a minimum value of stiffness is pre-set to prevent the stiffness from dropping continuously to zero when the τ_e is around a small value.

From Fig. 8 and Fig. 9, the interaction force is well estimated by VSA with higher accuracy in the process of human-robot interaction, and the robot is able to “actively” track the “motion intention” of human, thus providing a safe human-robot interaction.

V. DISCUSSIONS

This paper describes the controller for physical human-robot interaction for robots driven by VSA. The contributions can be highlighted as follows: (i) The interaction force is directly estimated by measuring the internal deflection of VSA, and the stiffness region control is developed to improve the performance of force estimation. (ii) The motion intention is achieved through the medium of interaction force, by estimating the limb model with only two unknown parameters to be updated, thus decreasing the computation cost.

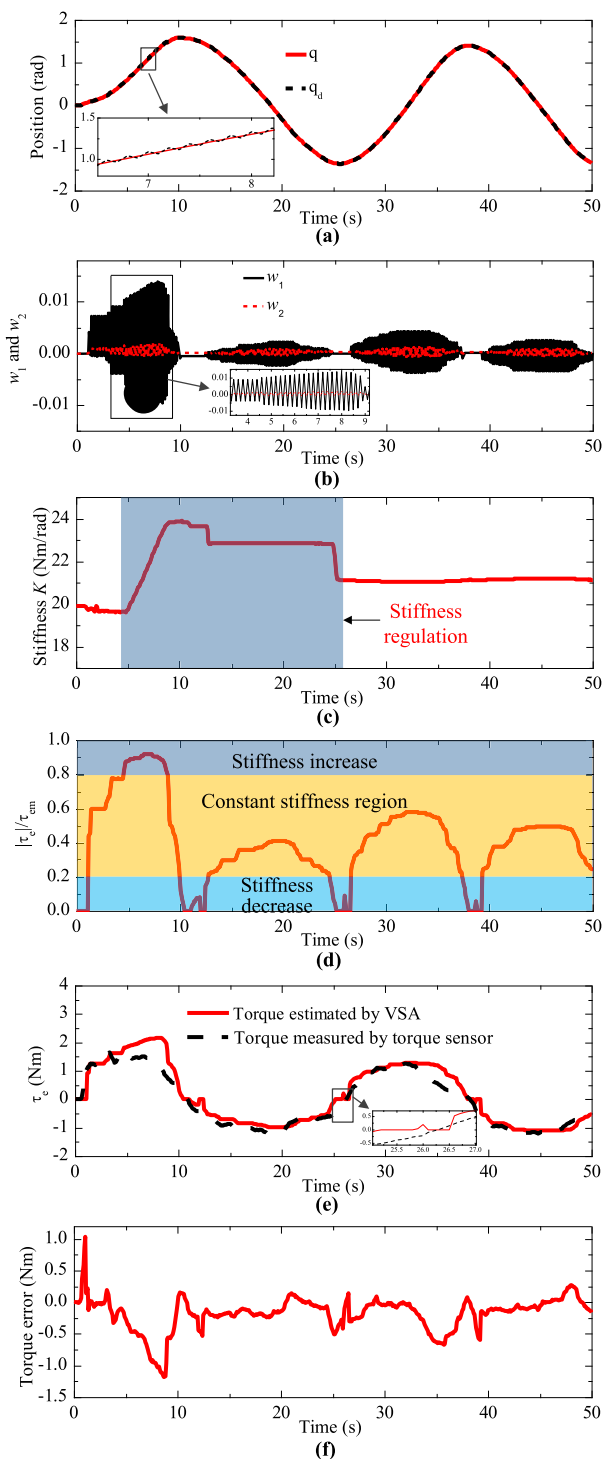


FIGURE 9. Experimental results with initial stiffness of $\alpha = \pi/18$.

Compared with the traditional methods of detecting the interaction force, the interaction force in this paper is directly estimated by detecting the internal deflection of VSA, which does not require additional force sensor or accurate dynamics. Besides, the stiffness region control is incorporated into the controller to achieve a proper resolution of force estimation and avoid violating the maximum internal

deflection simultaneously, which is difficult to be achieved for SEA.

In the estimation of motion intention, as the damper and spring variables of upper limb are all considered, the proposed method makes the estimation relatively accurate. Furthermore, unlike the [21] where the neural network was utilized, there are only two unknown parameters that are needed to be updated in this paper, thus contributing to a lower computation cost.

In Section III A, the constant stiffness region is the outcome of compromise between the resolution of force estimation and the allowable maximum force. It has the “proper” resolution of force estimation but not the “best” one. The resolution can be improved further by selecting the proper parameter η_1 .

In the experiment, the errors of torque estimation by VSA are smaller enough and acceptable for human-robot interaction. Such performance not only displays the effectiveness of the proposed stiffness region control, but also the accuracy of stiffness calibration in a dynamic condition.

From the experiments, when performing the cooperation task, the robot “actively” complies with the motion of human and provides certain resistance. Actually, the impedance parameters in (18) could be regulated for the interaction to achieve different degree of interaction force. Besides, even though the controller in this paper is only focusing on the robot with one DOF, such controller is easily extended to robots with multi-DOFs.

VI. CONCLUSION

In this paper, the control strategy for physical human-robot interaction has been investigated for robots driven by VSA. The interaction force is directly estimated by the internal deflection of VSA with the stiffness region control to improve the performance of force estimation. The human motion intention is estimated as the desired trajectory based on the estimated force, and then integrated into the impedance control to make the robot “actively” track the desired trajectory with compliance. Experiments have been carried out to verify the effectiveness of the proposed strategy. Such strategy can be readily extended to other robots driven by VSAs in the occasions involving human-robot cooperation.

REFERENCES

- [1] B. Vanderborght et al., “Variable impedance actuators: A review,” *Robot. Auton. Syst.*, vol. 61, no. 12, pp. 1601–1614, Aug. 2013.
- [2] S. Wolf, G. Grioli, O. Eiberger, W. Friedl, M. Grebenstein, H. Höppner, E. Burdet, D. G. Caldwell, R. Carloni, M. G. Catalano, D. Lefeber, S. Stramigioli, N. Tsagarakis, M. Van Damme, R. Van Ham, B. Vanderborght, L. C. Visser, A. Bicchi, and A. Albu-Schäffer, “Variable stiffness actuators: Review on design and components,” *IEEE/ASME Trans. Mechatronics*, vol. 21, no. 5, pp. 2418–2430, Oct. 2016.
- [3] X. Li, Y.-H. Liu, and H. Yu, “Iterative learning impedance control for rehabilitation robots driven by series elastic actuators,” *Automatica*, vol. 90, pp. 1–7, Apr. 2018.
- [4] H. Yu, S. Huang, G. Chen, Y. Pan, and Z. Guo, “Human–robot interaction control of rehabilitation robots with series elastic actuators,” *IEEE Trans. Robot.*, vol. 31, no. 5, pp. 1089–1100, Oct. 2015.
- [5] S. Mghames, M. Laghi, C. D. Santana, M. Garabini, M. Catalano, G. Grioli, and A. Bicchi, “Design, control and validation of the variable stiffness exoskeleton FLExo,” in *Proc. Int. Conf. Rehabil. Robot. (ICORR)*, London, U.K., Jul. 2017, pp. 539–546.
- [6] Y. Liu, S. Guo, H. Hirata, H. Ishihara, and T. Tamiya, “Development of a powered variable-stiffness exoskeleton device for elbow rehabilitation,” *Biomed. Microdevices*, vol. 20, no. 3, p. 64, Aug. 2018.
- [7] S. Li, J. Li, G. Tian, and H. Shang, “Stiffness adjustment for a single-link robot arm driven by series elastic actuator in muscle training,” *IEEE Access*, vol. 7, pp. 65029–65039, 2019.
- [8] C. D. Remy, R. Siegwart, C. Gehring, M. Bloesch, M. A. Hoepflinger, and M. Hutter, “StarLETH: A compliant quadrupedal robot for fast, efficient, and versatile locomotion,” in *Proc. 15th Int. Conf. Climbing Walking Robot*, 2012, pp. 1–8.
- [9] N. Paine, J. S. Mehling, J. Holley, N. A. Radford, G. Johnson, C.-L. Fok, and L. Sentis, “Actuator control for the NASA-JSC valkyrie humanoid robot: A decoupled dynamics approach for torque control of series elastic robots,” *J. Field Robot.*, vol. 32, no. 3, pp. 378–396, May 2015.
- [10] A. Ajoudani, J. Lee, A. Rocchi, M. Ferrati, E. M. Hoffman, A. Settini, D. G. Caldwell, A. Bicchi, and N. G. Tsagarakis, “A manipulation framework for compliant humanoid COMAN: Application to a valve turning task,” in *Proc. IEEE-RAS Int. Conf. Humanoid Robots*, Nov. 2014, pp. 664–670.
- [11] E. Basafa, M. Sheikholeslami, A. Mirbagheri, F. Farahmand, and G. R. Vossoughi, “Design and implementation of series elastic actuators for a haptic laparoscopic device,” in *Proc. Annu. Int. Conf. IEEE Eng. Med. Biol. Soc.*, Sep. 2009, pp. 6054–6057.
- [12] J. Oblak and Z. Matjačić, “Design of a series visco-elastic actuator for multi-purpose rehabilitation haptic device,” *J. Neuroeng. Rehabil.*, vol. 8, no. 1, pp. 1–13, Dec. 2011.
- [13] M. Cestari, D. Sanz-Merodio, J. C. Arevalo, and E. Garcia, “An adjustable compliant joint for lower-limb exoskeletons,” *IEEE/ASME Trans. Mechatronics*, vol. 20, no. 2, pp. 889–898, Apr. 2015.
- [14] M. K. Shepherd and E. J. Rouse, “The VSPA foot: A quasi-passive ankle-foot prosthesis with continuously variable stiffness,” *IEEE Trans. Neural Syst. Rehabil. Eng.*, vol. 25, no. 12, pp. 2375–2386, Dec. 2017.
- [15] J. Xu, Y. Liu, J. Chen, Y. Li, L. Xu, C. Peng, S. Chen, J. Liu, C. Xu, G. Cheng, and H. Xu, “A multi-mode rehabilitation robot with magnetorheological actuators based on human motion intention estimation,” *IEEE Trans. Neural Syst. Rehabil. Eng.*, vol. 27, no. 10, pp. 2216–2228, Oct. 2019.
- [16] P. W. Ferrez and J. del R. Millan, “Error-related EEG potentials generated during simulated brain–computer interaction,” *IEEE Trans. Biomed. Eng.*, vol. 55, no. 3, pp. 923–929, Mar. 2008.
- [17] W. Wang, Z.-G. Hou, L. Cheng, L. Tong, L. Peng, L. Peng, and M. Tan, “Toward patients’ motion intention recognition: Dynamics modeling and identification of iLeg—An LLRR under motion constraints,” *IEEE Trans. Syst., Man, Cybern. Syst.*, vol. 46, no. 7, pp. 980–992, Jul. 2016.
- [18] B. K. Dinh, M. Xiloyannis, C. W. Antuvan, L. Cappello, and L. Masia, “Hierarchical cascade controller for assistance modulation in a soft wearable arm exoskeleton,” *IEEE Robot. Autom. Lett.*, vol. 2, no. 3, pp. 1786–1793, Jul. 2017.
- [19] V. Duchaine, B. M. St-Onge, D. Gao, and C. Gosselin, “Stable and intuitive control of an intelligent assist device,” *IEEE Trans. Haptics*, vol. 5, no. 2, pp. 148–159, Apr. 2012.
- [20] C. Liang and T. Hsiao, “Admittance control of powered exoskeletons based on joint torque estimation,” *IEEE Access*, vol. 8, pp. 94404–94414, 2020.
- [21] Y. Li and S. S. Ge, “Human–robot collaboration based on motion intention estimation,” *IEEE/ASME Trans. Mechatronics*, vol. 19, no. 3, pp. 1007–1014, Jun. 2014.
- [22] C.-F. Chen, Z.-J. Du, L. He, Y.-J. Shi, J.-Q. Wang, G.-Q. Xu, Y. Zhang, D.-M. Wu, and W. Dong, “Development and hybrid control of an electrically actuated lower limb exoskeleton for motion assistance,” *IEEE Access*, vol. 7, pp. 169107–169122, 2019.
- [23] J. F. Veneman, R. Ekkelenkamp, R. Kruidhof, F. C. T. van der Helm, and H. van der Kooij, “A series elastic- and bowden-cable-based actuation system for use as torque actuator in exoskeleton-type robots,” *Int. J. Robot. Res.*, vol. 25, no. 3, pp. 261–281, Mar. 2006.
- [24] B. Huard, M. Grossard, S. Moreau, and T. Poinot, “Sensorless force/position control of a single-acting actuator applied to compliant object interaction,” *IEEE Trans. Ind. Electron.*, vol. 62, no. 6, pp. 3651–3661, Jun. 2015.
- [25] A. H. A. Stienen, E. E. G. Hekman, H. T. Braak, A. M. M. Aalsma, F. C. T. van der Helm, and H. van der Kooij, “Design of a rotational hydroelastic actuator for a powered exoskeleton for upper limb rehabilitation,” *IEEE Trans. Biomed. Eng.*, vol. 57, no. 3, pp. 728–735, Mar. 2010.

[26] B.-S. Kim and J.-B. Song, "Object grasping using a 1 DOF variable stiffness gripper actuated by a hybrid variable stiffness actuator," in *Proc. IEEE Int. Conf. Robot. Automat. (ICRA)*, Shanghai, China, May 2011, pp. 4620–4625.

[27] Y. Ning, H. Huang, W. Xu, W. Zhang, and B. Li, "Design and implementation of a novel variable stiffness actuator with cam-based relocation mechanism," *J. Mech. Robot.*, vol. 13, no. 2, Apr. 2021, doi: [10.1115/1.4049150](https://doi.org/10.1115/1.4049150).

[28] B.-S. Kim and J.-B. Song, "Design and control of a variable stiffness actuator based on adjustable moment arm," *IEEE Trans. Robot.*, vol. 28, no. 5, pp. 1145–1151, Oct. 2012.

[29] K. P. Tee, S. S. Ge, and E. H. Tay, "Barrier Lyapunov functions for the control of output-constrained nonlinear systems," *Automatica*, vol. 45, no. 4, pp. 918–927, Apr. 2009.

[30] M. M. Rahman, R. Ikeura, and K. Mizutani, "Investigation of the impedance characteristic of human arm for development of robots to cooperate with humans," *Int. J. C Mech. Syst., Mach. Elements Manuf.*, vol. 45, no. 2, pp. 510–518, 2002.



YINGHAO NING received the B.S. degree in mechanical design, manufacturing, and automation from the Taiyuan University of Science and Technology, Taiyuan, China, in 2013. He is currently pursuing the Ph.D. degree in mechanical engineering with the Harbin Institute of Technology, Shenzhen, China.

His research interests include the variable stiffness actuator and physical human–robot interaction.



YIFAN LIU received the B.S. degree in mechanical design, manufacturing, and automation from the Northwest A&F University, China, in 2018. He is currently pursuing the M.Sc. degree in mechanical and electronic engineering with the Harbin Institute of Technology, Shenzhen, China.

His research interests include structural design of robot complaint joints and mechanical modeling.



FENGFENG (JEFF) XI received the B.Eng. and M.Sc. degrees from Shanghai University, Shanghai, China, in 1982 and 1984, respectively, and the Ph.D. degree from the University of Toronto, Toronto, ON, Canada, in 1993.

He is currently a Professor with the Harbin Institute of Technology, Shenzhen, and also with the Department of Aerospace Engineering, Ryerson University, Toronto. His current research interests include sensor responsive design with application to smart aircraft cabins and aircraft manufacturing automation.



KE HUANG received the master's degree from the Inner Mongolia University of Technology, in 2013. He was a Guest Postgraduate with the Shenzhen Graduate School, Tsinghua University, and the Shenzhen Research Institute of Advanced Technology, Chinese Academy of Sciences, from September 2011 to July 2013.

He is currently working as a General Assistant Manager with Shenzhen Cansing Technology Company Ltd. He is also a Core Staff of the Phoenix team, Shenzhen. He has presided over or participated in six urban-level projects, published four papers, and obtained more than 40 patents.



BING LI (Senior Member, IEEE) received the Ph.D. degree in mechanical engineering from The Hong Kong Polytechnic University, Hong Kong, in 2001.

He has been a Professor of Mechatronics, since 2006. He is currently the Acting Dean of the School of Mechanical Engineering and Automation, Harbin Institute of Technology, Shenzhen, China. His current research interests include robotics, bionic robot, space agency, and mechanical vibration and control.

Dr. Li is an Associate Editor of the *Intelligent Service Robotics* and an Editorial Board Member of *Industrial Robot-The International Journal of Robotics Research and Application*.

...